Article

Incorporation of Fullerene Derivatives into Smectite Clays: A New Family of Organic–Inorganic Nanocomposites

Dimitrios Gournis, Vasilios Georgakilas, Michael A. Karakassides, Thomas Bakas, Konstantinos Kordatos, Maurizio Prato, Marianna Fanti, and Francesco Zerbetto

J. Am. Chem. Soc., **2004**, 126 (27), 8561-8568• DOI: 10.1021/ja049237b • Publication Date (Web): 18 June 2004

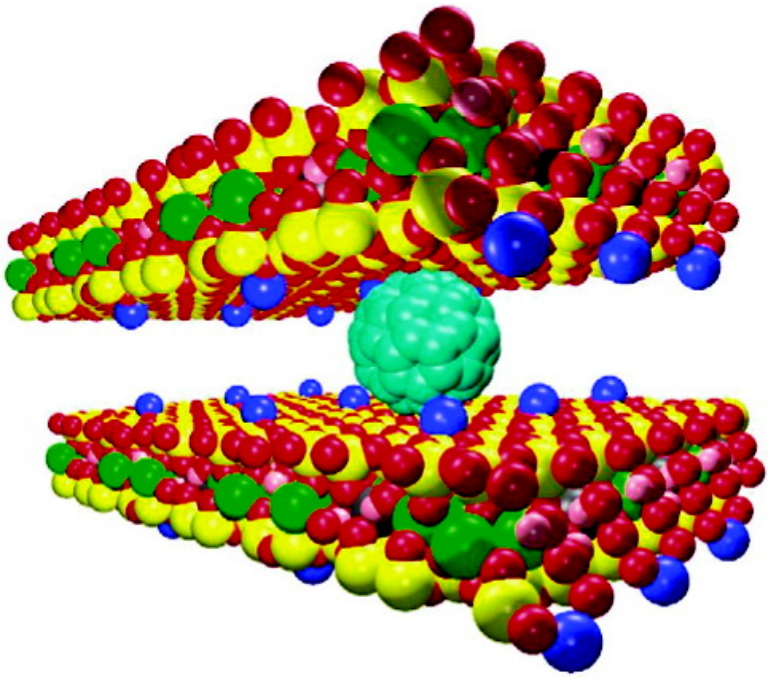

J|A|C|S
ARTICLES
Published on Web 06/18/2004

Incorporation of Fullerene Derivatives into Smectite Clays: A New Family of Organic−Inorganic Nanocomposites

Dimitrios Gournis,*,† Vasilios Georgakilas,‡ Michael A. Karakassides,† Thomas Bakas,§ Konstantinos Kordatos,|| Maurizio Prato,*,|| Marianna Fanti,⊥ and Francesco Zerbetto*,⊥

Contribution from the Departments of Materials Science and Engineering and Physics, University of Ioannina, 45110 Ioannina, Greece, Institute of Materials Science, NCSR "DEMOKRITOS", Ag. Paraskevi-Attikis, 15310 Athens, Greece, Dipartimento di Scienze Farmaceutiche, Università di Trieste, Piazzale Europa 1, 34127, Trieste, Italy, and Dipartimento di Chimica "G. Ciamician", Università di Bologna, V. F. Selmi 2, 40126 Bologna, Italy

Received February 12, 2004; E-mail: dgourni@cc.uoi.gr; prato@units.it; francesco.zerbetto@unibo.it

Abstract: Three fulleropyrrolidine derivatives, characterized by the presence of positive charges, were introduced in the interlayer space of montmorillonite. The composites were characterized by powder X-ray diffraction and differential thermal and thermogravimetric (DTA−TGA) analysis, in conjunction with FTIR, UV−Vis, Raman, and ^{57}Fe-Mössbauer spectroscopies. Organophilic derivatives were intercalated into organically modified clays, while water-soluble fulleropyrrolidines were introduced into the clay galleries through ion exchange. The experiments, complemented by computer simulations, show that not all the clay−clay platelets are intercalated by the fullerene derivatives and that a sizable amount of charge transfer takes place between the host and the guests.

Introduction

Fullerenes have been extensively studied during the past decade.[1,2] Their physical and chemical properties have been scrutinized, and a high number of organic derivatives and composites have been prepared and characterized. Drawbacks for their use in several applications, especially those based on optical and electronic properties, arise from their difficult processibility and incorporation into various solid matrixes such as polymers, glasses, metals, and other materials. Organic derivatization of fullerenes can help solubilization both in organic solvents and in water, and also adds or tunes their properties.[3]

Smectite clays are a class of layered aluminosilicate minerals with a unique combination of swelling, intercalation, and ion-exchange properties that make their nanostructures valuable in diverse fields.[4] They consist of an octahedral alumina layer fused between two tetrahedral silica layers. Such clays have a cation exchange capacity, which depends on the substitution of low-valent atoms, e.g., Mg^{2+} for Al^{3+} in the octahedral sheet and Al^{3+} for Si^{4+} in the tetrahedral sites. As a consequence, the layers have a fixed negative charge and neutrality is obtained, for example, by hydrated cations present in the galleries. The intercalation process in these systems is equivalent to ion exchange, and unlike the intercalation compounds of graphite, it does not involve necessarily charge transfer between the guest and host species. The charge on the layers affects many fundamental properties of the clays, including cation exchange capacity, cation fixation, swelling ability, water holding, and specific surface areas. These materials have the natural ability to adsorb organic or inorganic guest cationic species (and even neutral molecules) from solutions, and it is this cation "storage" that gives unique properties to clay minerals, which can be used as catalysts,[5] templates[6] in organic synthesis, or as components for composite materials.[7] The nature of the microenvironment between the aluminosilicate sheets regulates the topology of the

† Department of Materials Science and Engineering, University of Ioannina.
‡ Institute of Materials Science, NCSR "DEMOKRITOS".
§ Physics Department, University of Ioannina.
|| Università di Trieste.
⊥ Università di Bologna.

(1) See papers within: Special issue on *Functionalized Fullerene Materials*; Prato, M.; Martin, N., Guest Eds.; *J. Mater. Chem.* **2002**, *12* (7).
(2) (a) Prassides, K. *Physics and Chemistry of the Fullerenes*; Kluwer Academic: Dordrecht, The Netherlands, 1994. (b) Kroto, H. W. *The Fullerenes; New Horizons for the Chemistry, Physics and Astrophysics of Carbon*; Cambridge University Press: Cambridge, 1997. (c) Hirsch, A. *Fullerenes and Related Structures*; Springer: Berlin, 1999. (d) Kadish, K. M.; Ruoff, R. S. *Fullerenes: Chemistry, Physics and Technology*; Wiley-Interscience: New York, 2000. (e) Diederich, F.; Thilgen, C. *Science* **1996**, *271*, 317−323.
(3) (a) Prato, M. *J. Mater. Chem.* **1997**, *7*, 1097−1109. (b) Prato, M. *Top. Curr. Chem.* **1999**, *199*, 173−187. (c) Wudl, F. *J. Mater. Chem.* **2002**, *12*, 1959−1963.
(4) (a) Pinnavaia, T. J. *Science* **1983**, *220*, 365. (b) Konta, J. *Appl. Clay Sci.* **1995**, *10*, 275. (c) Lagaly, G. *Solid State Ionics* **1986**, *22*, 43. (d) Newman, A. C. D. *Chemistry of Clays and Clays Minerals*; Mineralogical Society Monograph, No. 6; Longman: London, 1987.
(5) (a) Ballantine, J. A. *NATO-ASI Ser., Ser. C* **1986**, *165*, 197. (b) Cornelis, A.; Laszlo, P. *NATO-ASI Ser., Ser. C* **1986**, *165*, 213.
(6) (a) Georgakilas, V.; Gournis, D.; Bourlinos, A. B.; Karakassides, M. A.; Petridis, D. *Chem.−Eur. J.* **2003**, *9*, 3904. (b) Georgakilas, V.; Gournis, D.; Petridis, D. *Angew. Chem., Int. Ed.* **2001**, *40*, 4286. (c) Bourlinos, A. B.; Petridis, D. *J. Inclusion Phenom. Macrocyclic Chem.* **2001**, *40*, 147.
(7) (a) Theng, B. K. G. *The Chemistry of Clay-Organic Reactions*; Adam Hilger: London, 1974. (b) Kloprogge, J. T. *J. Porous Mater.* **1998**, *5*, 5. (c) Gil, A.; Gandia, L. M. *Catal. Rev.−Sci. Eng.* **2000**, *42*, 145. (d) Ma, Y.; Tong, W.; Zhou, H.; Suib, S. L. *Microporous Mesoporous Mater.* **2000**, *37*, 243. (e) Ohtsuka, K. *Chem. Mater.* **1997**, *9*, 2039. (f) Shichi, T.; Takagi, K. *J. Photochem. Photobiol., C* **2000**, *1*, 113−130.

Scheme 1. The Three Fullerene Derivatives

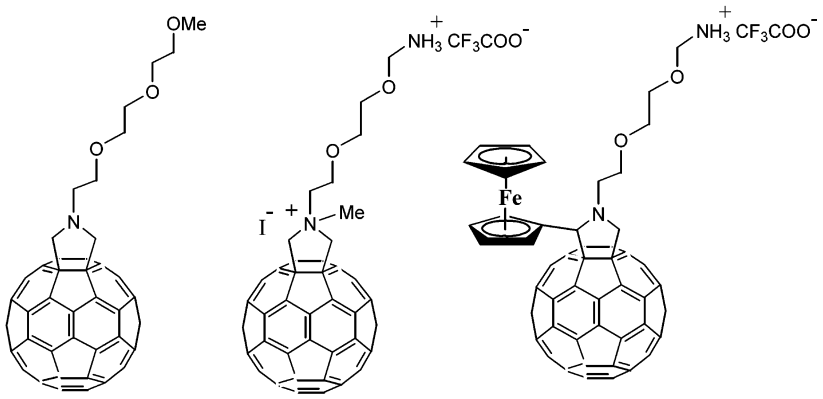

FD1 **FD2** **FD3**

intercalated molecules and affects possible supramolecular rearrangements or reactions, such as self-assembling processes that are usually not easily controlled in the solution phase.[7]

The incorporation of C_{60} into porous or layered materials is a nontrivial task, and the study of these composites can offer helpful answers about the utilization of fullerenes and their derivatives for possible applications. In addition, it can be examined whether fullerene derivatives can form novel structures, where the molecules are ordered in one or two dimensions, and how the presence of a molecule changes the basic properties of the bulk material. Moreover, the C_{60}-based organic/clay hybrid materials may possess interesting photophysical characteristics and thus may enable the development of photofunctional devices in the form of anisotropic thin films on metallic or glass surfaces.[7f]

A further challenging goal is the possibility to direct C_{60} functionalization using the clays. The 30 formal double bonds of C_{60} can be easily functionalized in many types of organic reactions. The presence of so many reacting bonds creates numerous isomers and increases the difficulties in the separation and characterization of the products. However, when a fullerene is placed between the clay layers, a part of the surface cage is protected and some double bonds become inactive to any reaction. The interlayer space of clay is therefore expected to induce selective reactivity, but it may also be interesting to study the fullerene reactivity in a microenvironment such as that of the interior of the clay.

Finally, fullerene derivatives grafted to aluminosilicate layers are attractive for polymer reinforcing applications. One would expect that the combined action of clay and fullerene derivatives in polymer matrixes could provide novel functionalities to the resulting composite materials. In particular, the inherent electrical properties of C_{60} as a component of polymer composites could produce materials with enhanced static dissipation, better electromagnetic compatibility, and improved thermal conductivity.

The incorporation of C_{60} into molecular sieves, layered double hydroxides (LDH), and mica-type silicates has been studied. Keizer et al.[8] reported the trapping of C_{60} in 13× molecular sieves through gas-phase absorption and the occurrence of C_{60}^- radical ions. Hamilton et al.[9] reported the incorporation of C_{60} into channel-shape porous sieves VPI-5 from benzene solutions. The composite showed strong white light emission arising from the C_{60} molecules. Giannelis et al.[10] incorporated water-soluble ethylenediamine-functionalized fullerene into mica-type silicate layers through ion exchange. Finally, Cheng et al.[11] reported the incorporation of pure C_{60} into LDH with dodecyl sulfate counterions and noted that the C_{60} molecules do not rotate as freely as those in the pure solid form.

In this work, we report the successful incorporation of fulleropyrrolidine derivatives into hydrophilic or modified organophilic clays by ion exchange or organic solution, respectively. The clay/fulleropyrrolidine composites have been characterized by powder X-ray diffraction and differential thermal and thermogravimetric (DTA−TGA) analysis, in conjunction with FTIR, UV−Vis, Raman, and ^{57}Fe-Mössbauer spectroscopies. The experiments reveal the inherent complexity of these materials but leave some open questions that are addressed by computer simulations.

Experimental Section

Host Layered Material. The clay used was a natural Wyoming sodium montmorillonite (SWy-1) obtained from the Source Clay Minerals Repository, University of Missouri (Columbia, MO), with a cation exchange capacity (CEC) measured by the Co(II) procedure equal to 80 mequiv per 100 g clay. The clay was fractioned to <2 μm by gravity sedimentation and purified by well-established procedures in clay science. Sodium-exchanged samples (Na^+−MNT) were prepared by immersing the clay into 1 N solution of sodium chloride. Cation exchange was completed by washing and centrifuging four times with dilute aqueous NaCl. The samples were finally washed with distilled−deionized water and transferred into dialysis tubes to obtain chloride-free clays and then dried at room temperature.

Synthesis of Fulleropyrrolidine Derivatives. The three fullerene derivatives (see Scheme 1), referred to here as **FD1**, **FD2**, and **FD3**, were prepared according to the literature.[12]

Preparation of Organoclay Substrates and Intercalation of Neutral FD1 Derivative. To prepare the organoclay, a solution of the surfactant (trimethyl-hexadecylammonium chloride) in water (1.2 CEC) was added to a stirred clay suspension of Na^+−MNT (100 mg) in water

(8) Keizer, P. N.; Morton, J. R.; Preston, K. F.; Sugden, A. K. *J. Phys. Chem.* **1991**, *95*, 7117.

(9) (a) Hamilton, B.; Rimmer, J. S.; Anderson, M.; Leigh, D. *Adv. Mater.* **1993**, *5*, 583. (b) Anderson, M. W.; Shi, J.; Leigh, D. A.; Moody, A. E.; Wade, F. A.; Hamilton, B.; Carr, S. T. *J. Chem. Soc., Chem. Commun.* **1993**, 533.

(10) Mehrotra, V.; Giannelis, E. P. *Chem. Mater.* **1992**, *4*, 20−22.

(11) Tseng, W. Y.; Lin, J. T.; Mou, C. Y.; Cheng, S.; Liu, S. B.; Chu, P. P.; Liu, H. W. *J. Am. Chem. Soc.* **1996**, *118*, 4411−4418.

(12) Kordatos, K.; Da Ros, T.; Bosi, S.; Vazquez, E.; Bergamin, M.; Cusan, C.; Pellarini, F.; Tomberli, V.; Baiti, B.; Pantarotto, D.; Georgakilas, V.; Spalluto, G.; Prato, M. *J. Org. Chem.* **2001**, *66*, 4915−4920.

(3 mL). The mixture was stirred, centrifuged, washed with water three times, and air-dried. The dry powder was dispersed in chloroform (5 mL) and stirred overnight. A solution of FD1 in toluene (5 mg in 5 mL) was added, and the mixture was stirred overnight. The clay was collected by centrifugation and washed by chloroform several times to remove any residue attached or crystallized on the external surfaces of the clay and finally air-dried.

Preparation of Clay/Fullerene Derivatives (FD2 and FD3) Composites. A saturated brown-colored water solution of 25 mg of FD2 in water was mixed with a suspension of 100 mg of Na^+−MNT in 50 mL of distilled water. The mixture was stirred at room temperature for 2 to 3 h until no color was observed at the supernatant. The residue, separated by centrifugation, was washed several times by water and air-dried over a glass plate (**clay/FD2** product). Fulleropyrrolidine FD3 was only slightly soluble in water, and thus, 2 mL of DMSO was added in the water solution of FD3 to increase the solubility. The solution of FD3 was then mixed with 100 mg Na^+−MNT in 50 mL of distilled water. **Clay/FD3** composite was also prepared according to the previous procedure.

Characterization Techniques. The X-ray powder diffraction patterns were collected using Cu Kα (40 kV, 40 mA) radiation and a secondary beam graphite monochromator. The patterns were recorded in the 2-theta (2Θ) range from 2° to 80°, in steps of 0.02° and counting time 2 s/step. Infrared spectra were measured in the region of 400−4000 cm^{-1}, and each spectrum was the average of 200 scans collected at 2 cm^{-1} resolution. Samples were in the form of KBr pellets containing ca. 2 wt % sample. Raman spectra were recorded using a laser excitation line at 532 nm (Nd:YAG). A 0.5 to 1 mW was used with 1 μm focus spot to avoid photodecomposition of the samples with a resolution 1 cm^{-1}. Transmission UV−Vis spectra on liquid samples were obtained by dissolving the samples in toluene or cyclohexane. For thermogravimetric (TGA) and differential thermal (DTA) analyses, samples of approximately 10 mg were heated in air from 25 to 700 °C at a rate of 5 °C/min. Mössbauer measurements were carried out with a conventional constant acceleration spectrometer equipped with a ^{57}Co(Rh) source calibrated with α-Fe, and isomer shift values are reported relative to this. The spectra, recorded at 30 K, were fitted on a PC with a least-squares minimization procedure assuming Lorentzian line shapes.

Results and Discussion

The incorporation of organic molecules into the interlayer space of layered aluminosilicates usually follows two main pathways. Positively charged molecules are introduced into the interlayer space of layered clay mineral by a simple ion-exchange procedure. Charge-balancing cations, e.g., Na^+, are replaced easily by the organic cations, and this is, in general, an easy and convenient method for the intercalation of organic cations soluble in water into the lamellar space of clay minerals. The newly introduced organic cations are held strongly by electrostatic forces between the large organic cations and the negatively charged clay surfaces, and the final conformation depends on the shape, size, and total charge of the organic cations and also on the charge density of the clay surface. More specifically, in the case of alkylammonium cations, the amine function ($-NH_3^+$) is exchanged on the exchangeable sites of the clay layer and the organic tail of the molecule lies horizontally or takes an inclined position between the clay layers. The introduction of organic cations increases the organophilicity of the clay mineral and produces organoclays, which are now dispersed in organic solvents. Alternatively, neutral organic molecules (soluble in water) could also be intercalated into the clay layers without removal of the exchangeable cations, and in this case, the molecules are trapped into the inorganic layers through van der Waals interactions between the organic molecules and the siloxane surface. In this case, the organic molecules are weakly held between the clay layers, and consequently, the quantity of adsorbed molecules is low. The use of organoclays, dispersed in organic solvents, instead of raw minerals, increases the amount of adsorbed organic molecules.

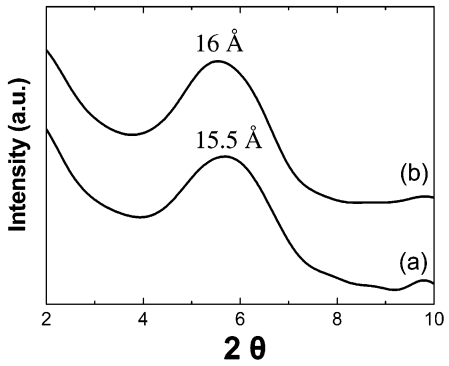

Figure 1. XRD diffraction patterns of (a) organoclay and (b) organoclay/FD1 composite.

In the first part of our work, Na^+ exchangeable cations were replaced by a cationic surfactant to enhance the organophilicity of the clay. As a consequence, the interlayer space was expanded because of the size and the conformation of the organic cations. Thus, organic solvents such as toluene or chloroform could enter into the clay galleries, transferring, in this way, the neutral fulleropyrrolidine molecules. X-ray diffraction measurements represent a powerful way to understand the changes in the interior of the clay microenvironment, since the interlayer distance can be estimated by measuring the d_{001} spacing. The powder XRD patterns of organoclay and organoclay-FD1 composite are shown in Figure 1. The initial insertion of the organic surfactant into the clay interlayer expanded the distance between the layers, giving a d_{001} value of 15.5 Å, which corresponds to an intersheet separation of $\Delta = 15.5 - 9.6 = 5.9$ Å, where the value of 9.6 Å represents the thickness of the clay sheet. This value implies that the flexible alkyl groups of the cationic surfactant must adopt an inclined position between the clay surfaces. The organic surfactant keeps the interlayer space expanded and helps the organic solvents to penetrate. The insertion of chloroform expanded even more the distance between the layers, and subsequently a neutral fulleropyrrolidine (FD1) entered easily and remained embedded, even after evaporation of chloroform. After the insertion of the fullerene derivative, the distance was not remarkably altered ($d_{001} = 16$ Å) since the size of the fullerene core is similar to the interlayer space of the organoclay. A possible schematic representation of the arrangement of intercalated fullerene derivatives in organoclay is shown in Scheme 2a. Fullerene derivatives probably sit between the organic surfactants and are trapped in the interlayer space through van der Waals interactions of the hydrophobic portion of the organic fullerene with the alkyl chains of the surfactants. The insertion of FD1 did not cause any change in the IR spectrum of organoclay (not shown) since the amount of the intercalated molecules and the expected bands are not sufficient to alter the intensity of the original peaks. An overnight treatment of organoclay/FD1 with a solution of LiCl resulted in the removal of the organic surfactant from the clay and its substitution by Li^+ cation as evidenced by infrared spectroscopy where the peaks that remained were only due to

Scheme 2. Schematic Representation of the Arrangement of Intercalated FD1 in Organoclay (a) and Possible Orientation of Fullerene Derivatives FD2 (b) and FD3 (c) into the Clay Interlayers

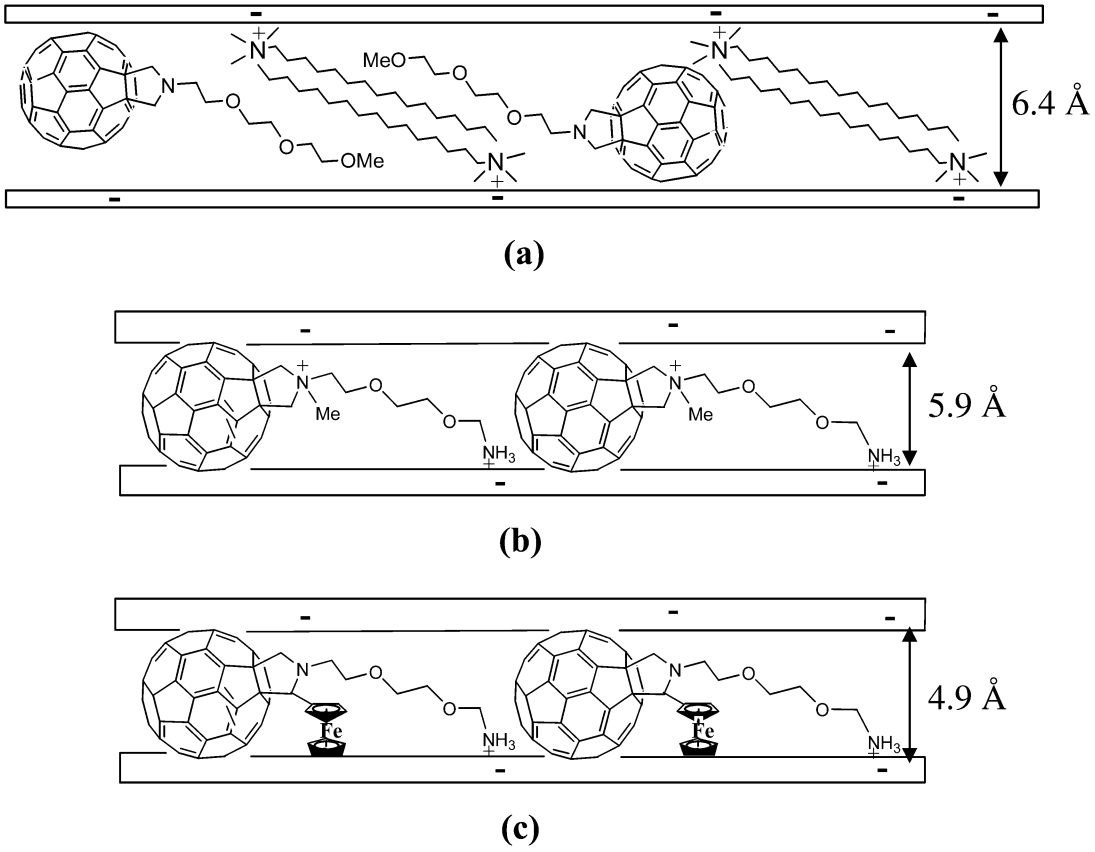

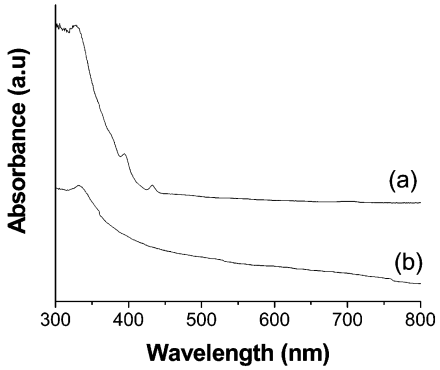

Figure 2. UV−vis spectra of (a) FD1 and (b) organoclay/FD1 in toluene.

the FD1. The derived composite Li−MNT/FD1 has a d_{001} value of 15.6 Å, which can be attributed to the size of the fullerene core. Another piece of important information derived from the XRD pattern of organoclay/FD1 was the absence of reflection peaks of the crystaline phase of FD1 in the 2θ region 2−80°. This indicates that FD1 molecules were not aggregated on the external clay surfaces after washing the product with chloroform.

The presence of FD1 in the final composite material was confirmed by UV−Vis spectroscopy. Fulleropyrrolidines have a characteristic UV−Vis absorption spectrum, as shown in Figure 2a, which consists of a narrow strong band at 326 nm and two weak peaks at 395 and 432 nm. The absorption spectrum of intercalated FD1 (Figure 2b) is now broader, with the main strong band red-shifted by 6 nm (to 332 nm) as compared to toluene solution of FD1. This result is in agreement with absorption studies in various media, which have shown a tendency for the main absorption peaks to be red-shifted when fullerene is isolated at the vicinity of polar interfaces.[13,14]

The incorporation of fulleropyrrolidines into the interlayer space of unmodified clay (Na^+−MNT) was carried out also using fullerene derivatives FD2 and FD3, positively charged and slightly soluble in water. In this case, unmodified clay could be used to simplify the procedure. When Na^+−MNT suspended in water was mixed with a brown-colored water solution of the ionic fulleropyrrolidine FD2, the supernatant became colorless after being stirred at room temperature for 2 h, indicating a successful and fast exchange. FD3 was not soluble enough in water, and therefore DMSO was used to solubilize it.

Figure 3a,c shows the XRD diffraction patterns of clay/FD2 and clay/FD3 composites. The introduction of FD2 increases the d_{001} spacing of the clay mineral from 12.3 in the pristine Na^+−MNT to 15.5 Å, which corresponds to an intersheet separation of 5.9 Å. This value is not in full agreement with the size of C_{60} (∼7 Å). Similarly, the XRD pattern of clay/FD3 showed a d_{001} spacing of 14.5 Å, which corresponds to an intersheet separation of 4.9 Å. This phenomenon may have two different explanations. (i) The fullerene cage is affected by the interaction with the clay sheets and becomes pancakelike (in turn, this could result in modified optical properties of the functionalized fullerene. While the presence of the inorganic sheets makes the investigation of the optical properties difficult, we plan to pursue this in further work). (ii) More likely, the

(13) Lamrabte, A.; Janot, J. M.; Elmidaoui, A.; Seta, P.; de Menorval, L. C.; Bancov, R.; Roziere, J.; Sauvajov, J. L.; Allegre, J. *Chem. Phys. Lett.* **1998**, *295*, 257−265.
(14) Sariciftci, N. S.; Smilowitz, L. S.; Heeger, A. J.; Wuld, F. *Synth. Met.* **1993**, *59*, 333.

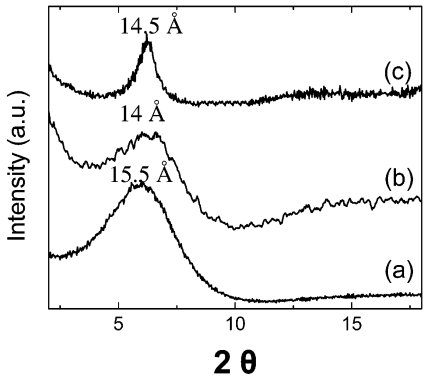

Figure 3. XRD diffraction patterns of (a) MNT/FD2, (b) MNT/FD2 after heating at 300 °C for 24 h under argon, and (c) MNT/FD3.

simplest explanation is the existence of filled and unfilled silicate layers, which results in a lower intersheet separation than expected.

The possible orientations of FD2 and FD3 between the clay layers are depicted in Scheme 2b,c. After heating the clay/FD2 sample to 300 °C for 24 h in argon atmosphere, the aliphatic chains were removed as indicated by the IR spectra (see below). The XRD pattern (Figure 3b) showed a small decrease to d_{001} = 14 Å, and this indicates a possible reaction between the fullerene spheres.

The IR spectrum of the clay/FD2 (Figure 4a) contains the characteristic peaks from the FD2 and also from the clay, without significant changes, confirming the presence of the fullerene derivative in the clay mineral. Clay/FD2 shows peaks at 3628 (clay lattice −OH stretching vibrations), 3418 (adsorbed H_2O deformation), 2921 and 2852 ($-CH_2-$, $-CH_3$ stretching vibrations of fullerene organic chain), 1633 (H_2O bending), 1459 and 1426 ($-CH_2-$, $-CH_3$, and −NH bending vibrations), and 1042 cm^{-1} (clay lattice Si−O and Si−O−Si vibrations). A similar spectrum was recorded for clay/FD3 (not shown), which showed peaks at 2927, 2866, 1526, 1458, and 1042 cm^{-1}. The characteristic peak due to the ferrocene moiety, at 3080 cm^{-1}, was not visible since it was covered by the intense band at 3200 cm^{-1}. After heat treatment of clay/FD2 to 300 °C, the side chains of the molecules were removed as evidenced by the absence of the characteristic vibrations of $-CH_2-$ and $-CH_3$ at 2800−2950 cm^{-1} (Figure 4b).

Figure 5 shows the DTA−TGA curves, under air, of the composite clay/FD2 in comparison with that of pure FD2 and montmorillonite clay separately. Montmorillonite clay showed a 15% weight loss until 150 °C, which is related to the removal of the intercalated water due to evaporation. On the other hand, pure FD2 showed approximately 20% weight loss between 150 and 220 °C, 20% between 250 and 420 °C, and 60% between 420 and 550 °C. Considering the mass percentage, these signals could correspond to the removal of I^- and CF_3COO^-, the aliphatic chain, and the rest of the molecule, respectively. Similar analysis of clay/FD2 composite showed that the intercalated FD2 was 30% of the total mass. The weight loss steps were not as defined as in the separated components. However, the DTA analysis showed that the first exothermal reaction, which probably corresponds to the removal of the aliphatic chain, occurs at lower temperature as compared to pure FD2, whereas the second exothermic step (C_{60} oxidation) occurred at similar temperature as before. Analogous results were obtained for the

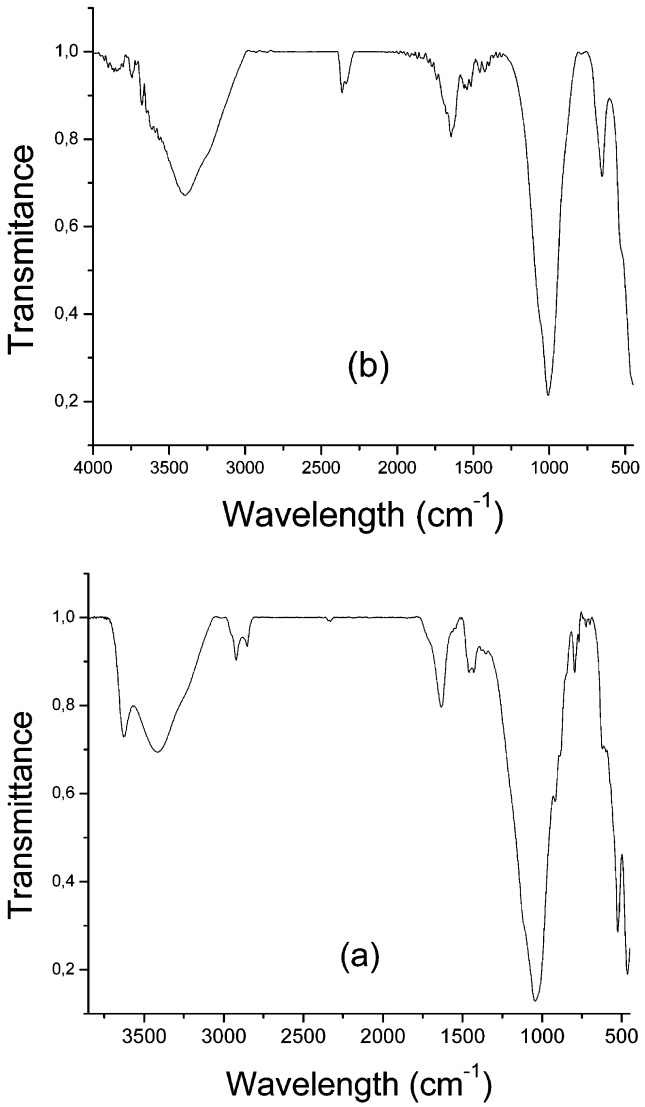

Figure 4. FT-IR spectra of (a) clay/FD2 and (b) after removal of aliphatic chains by heating the clay/FD2 composite at 300 °C in argon atmosphere.

clay/FD3 composite. In this case, the fullerene derivative corresponds to about 25 wt % of the total mass.

Raman spectroscopy was used to identify the existence of fullerene derivatives in the composite material. It is well-known that the vibrational modes of the isolated C_{60} (I_h point group) molecule have 10 Raman active bands: 2 with A_g symmetry and 8 with H_g symmetry.[15,16] The molecule has also four IR-active bands of F_{1u} symmetry and 32 IR and Raman forbidden bands corresponding to the $1A_u$, $3T_{1g}$, $4T_{2g}$, $5T_{2u}$, $6G_g$, $6G_u$, and $7H_u$ symmetry species. As shown in Figure 6, the Raman spectrum of pure C_{60} exhibits the strongest bands at 1467 and 493 cm^{-1} (A_g symmetry) and a number of weaker bands at 707, 770, 1248, 1420, 1490, and 1571 cm^{-1} (H_g symmetry). After modification, the spectrum of pure fullerene derivative FD2 changes drastically. More specifically, the dominant band at 1467 cm^{-1} of $A_g(2)$ symmetry is downshifted by approximately 7 cm^{-1}, whereas the 493 cm^{-1} band of $A_g(1)$ almost disappears. These changes were accompanied by the appearance of ad-

(15) Schettino, V.; Pagliai, M.; Ciabini, L.; Cardini, G. *J. Phys. Chem. A* **2001**, *105*, 11192−11196.
(16) Negri, F.; Orlandi, G.; Zerbetto, F. *Chem. Phys. Lett.* **1988**, *144*, 31−37.

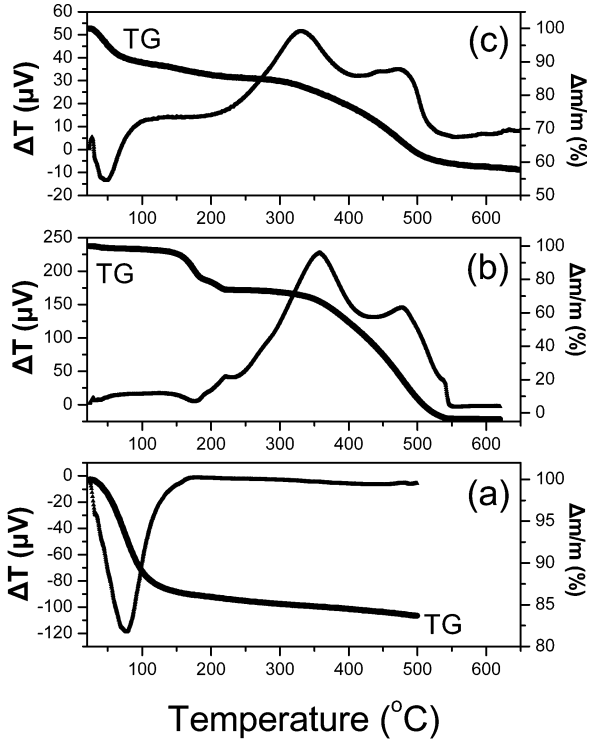

Figure 5. DTA−TGA curves of (a) Na^+−MNT, (b) pure FD2, and (c) clay/FD2 composite.

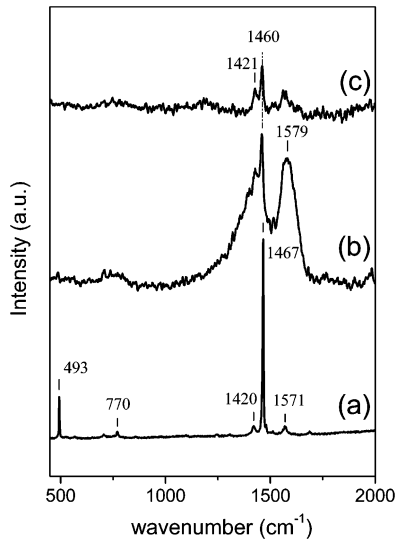

Figure 6. Raman spectra of (a) pure C_{60}, (b) pure FD2, and (c) clay/FD2 composite.

ditional Raman bands centered at 1420 and 1579 cm^{-1} (strong and broad) and around 750, 1770, and 1970 cm^{-1} (weak and broad). All these spectral changes suggest the formation of fulleropyrrolidine derivative FD2. For instance, the observed shift of 7 cm^{-1} in A_g mode could be attributed to fullerene modification during the preparation of the FD2 composite, since the A_g mode of C_{60} is sensitive to chemical modification.[17,18] Similar downshift has been observed in the Raman spectra of TDAE-C_{60} single crystals (TDAE is tetrakis (dimethyl-amino) ethylene)[18d] in comparison with the spectrum of pure C_{60}, in

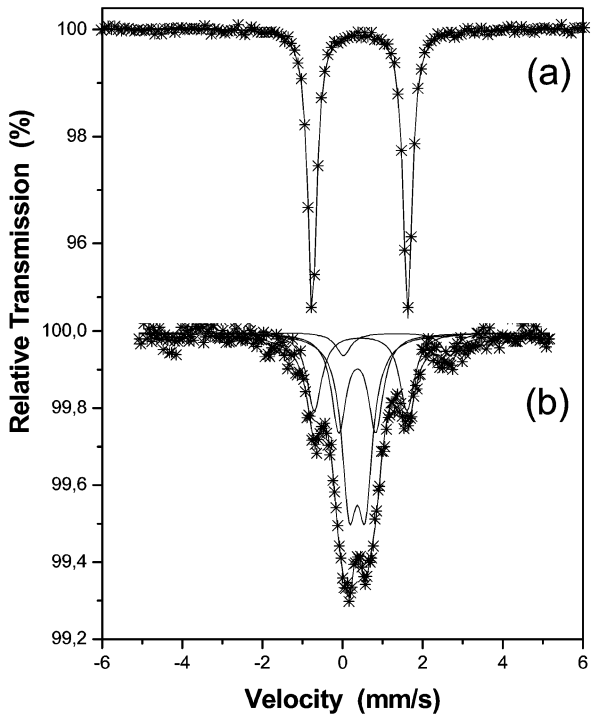

Figure 7. Mössbauer spectra, at 30 K, of (a) pure FD3 and (b) clay/FD3 composite.

the spectra of C_{60} fullerene photopolymers,[18c] in charge-transfer C_{60} complexes with tetraphenylphosphonium halides,[18a] in samarium−fullerence intercalation compounds,[18b] etc. In addition, the new and broad bands in the spectrum of FD2 composite (Figure 6b) could be attributed to distortion of C_{60} molecules as their symmetry is reduced in that of fulleropyrrolidine derivatives, resulting in the splitting of various degenerate modes and the activation of some silent modes. Thus, in agreement with previous studies on other C_{60} derivatives,[18] we can assign the new observed Raman bands in the spectrum of FD2 derivative to silent modes of C_{60} which became active after modification. On the other hand, in the spectrum of clay/FD2 composite (Figure 6c) the only well observable peaks are those around 1460, 1421, and 1570 cm^{-1}. The existence of these peaks in the Raman spectrum clearly proves the successful intercalation of FD2 inside the clay layers. Thus, the Raman measurements reveal the modification of C_{60} and the intercalation of the new functionalized derivative inside the clay layers.

Since the FD3 sample contains a ferrocene group, ^{57}Fe-Mössbauer spectroscopy was applied to reveal the existence of the fullerene derivative in the clay composite. The spectra of the FD3 and clay/FD3 samples, at 30 K, are shown in Figure 7. The spectrum of the FD3 sample consists of one doublet, and the hyperfine parameters of the ferrocene group are the same as those reported in the literature (isomer shift, $\delta = 0.54$ mm/s, and quadrupole splitting, $\Delta E_q = 2.38$ mm/s).[19] The spectrum of the clay/FD3 sample consists of four superimposed doublets. Three of them are characteristic of iron sites present in the clay structure: two corresponding to trivalent iron attributed to cis

(17) (a) Wang, K. A.; Wang, Y.; Zhou, P.; Holden, J. M.; Ren, S. L.; Hager, G. T.; Ni, H. F.; Eklund, P. C.; Dresselhaus, G.; Dresselhaus, M. S. *Phys. Rev. B* **1992**, *45*, 1995. (b) Talyzin, A. V.; Jansson, U. *Thin Solid Films* **2003**, *429*, 96−101.

(18) (a) Sauvajol, J. L.; Graja, A.; Firlej, L.; Król, S. *J. Mol. Struct.* **1997**, *436*−*437*, 19−23. (b) Wang, Y.; Cao, X.; Han, H. U.; Lan, G. *J. Phys. Chem. Solids* **2002**, *63*, 2053−2056. (c) Cataldo, F. *Eur. Polym. J.* **2000**, *36*, 653−656. (d) Pokhodnia, K.; Demsar, J.; Omerzu, A.; Mihailovic, D.; Kuzmany, H. *Synth. Met.* **1997**, *85*, 1749−1750.

(19) Wertheim, G. K.; Herber, R. H. *J. Phys. Chem.* **1963**, *38*, 2106−2111.

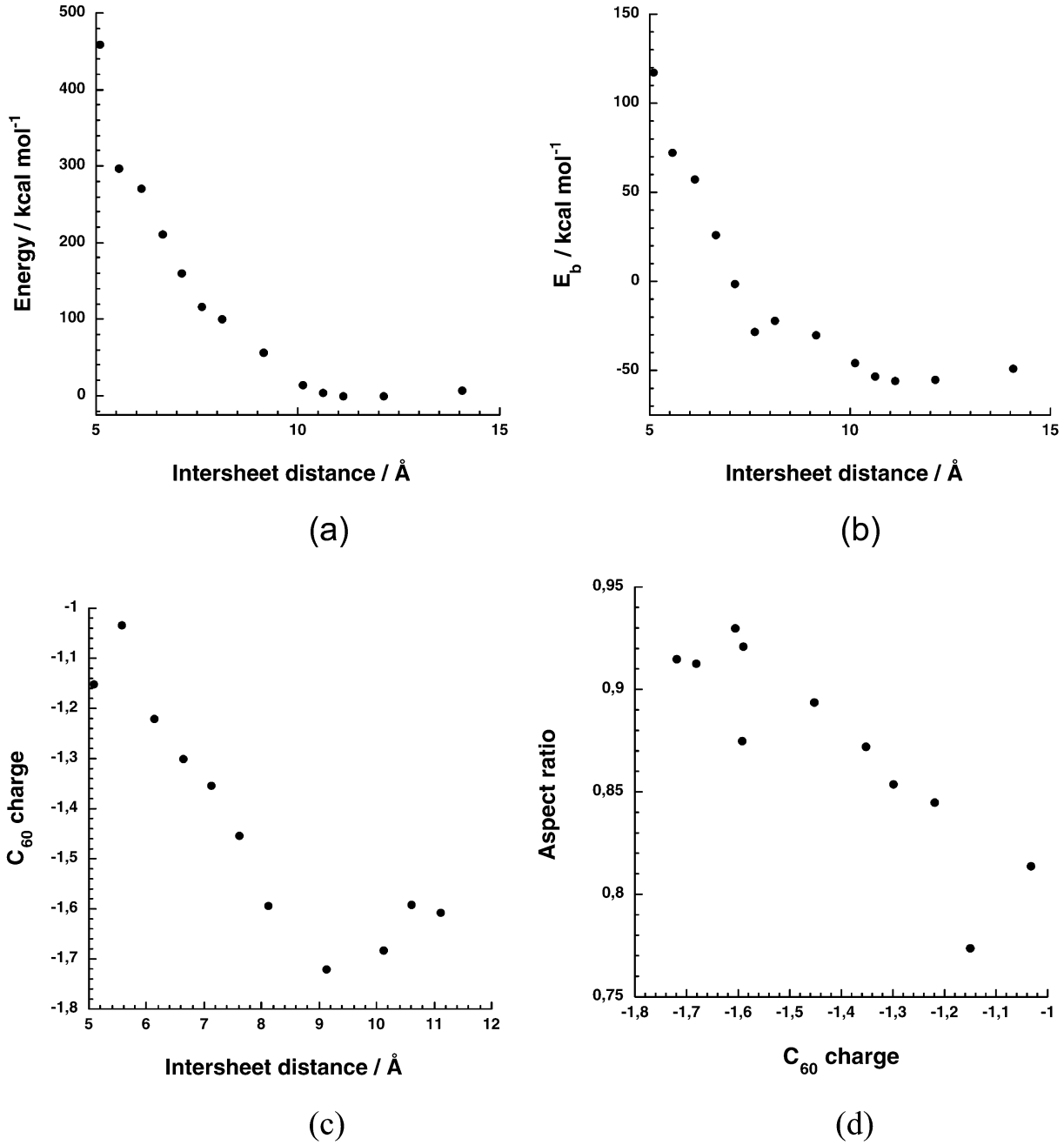

Figure 8. (a) Calculated energy variation with the intersheet distance. The region around the minimum is rather flat and is located at ~11 Å. (b) C_{60} binding energy as a function of the intersheet distance. (c) C_{60} charge as a function of the intersheet separation. (d) C_{60} charge as a function of the molecule aspect ratio.

and trans arrangement of the two hydroxyl groups [$FeO_4(OH)_2$] in the octahedral layer and a third corresponding to divalent iron in octahedral coordination, too.[20] The fourth doublet is the same as that for the FD3 sample, indicating the existence of the ferrocene group and consequently the FD3 derivative in the composite material.

As a partial summary, one can conclude that the experimental results show that the incorporation of fullerene derivatives into the aluminosilicate layers can be successfully achieved and that the fullerene derivatives are very strongly held between the inorganic sheets.

Simulations can contribute to address some of the experimental issues. Here we adopt a molecular mechanics force field that was used by some of us before[21] and was implemented by us in the TINKER package,[22] which has found several applications in one of our laboratories.[23] The brute formula of the elementary cell was $Na[(Si_{16})(Al_7Mg)O_{40}(OH)_8]$. The only

(20) Gournis, D.; Mantaka-Marketou, A. E.; Karakassides, M. A.; Petridis, D. *Phys. Chem. Miner.* **2000**, *27*, 514−521.

(21) Cavallini, M.; Lazzaroni, R.; Zamboni, R.; Biscarini, F.; Timpel, D.; Zerbetto, F.; Clarkson, G. J.; Leigh, D. A. *J. Phys. Chem. B* **2001**, *105*, 10826−10830.

(22) (a) Ponder, J. W.; Richards, F. J. *J. Comput. Chem.* **1987**, *8*, 1016. (b) Kundrot, C.; Ponder, J. W.; Richards, F. J. *J. Comput. Chem.* **1991**, *12*, 402. (c) Dudek, M. J.; Ponder, J. W. *J. Comput. Chem.* **1995**, *16*, 791.

(23) (a) Biscarini, F.; Cavallini, M.; Leigh, D. A.; León, S.; Teat, S. J.; Wong, J. K. Y.; Zerbetto, F. *J. Am. Chem. Soc.* **2002**, *124*, 225−233. (b) Georgakilas, V.; Pellarini, F.; Prato, M.; Guldi, D. M.; Melle-Franco, M.; Zerbetto, F. *Proc. Natl. Acad. Sci. U.S.A.* **2002**, *99*, 5075−5080. (c) Teobaldi, G.; Zerbetto, F. *J. Am. Chem. Soc.* **2003**, *125*, 7388−7393. (d)

atomic substitutions considered were Mg/Al (no Si/Al or Fe substitution). Periodic boundary conditions were applied, and the geometry was optimized with the only constraints of fixed OH distances and fixed *c* axis of the cell. The typical clay simulation cell—not the unit cell—contained 1458 plus C_{60} (see Figure S1 in the Supporting Information). The parameters were $a = 30.72$ Å, $b = 53.754$ Å, $c =$ dependent on the simulation, $\alpha = 90.0$, $\beta = 99.1$, and $\gamma = 90.0$. The *c* axis was varied in different simulations, but was kept constant for a given simulation to modify the intersheet separation. In practice, the simulation box contains only one clay platelet plus C_{60}, the second clay layer is introduced by the periodic boundary conditions.

The calculations investigated:

(i) The origin of the small intersheet distance.

(ii) The size of the C_{60}–clay interaction energy.

(iii) The origin of the frequency shift of the $A_g(2)$ mode.

Figure 8a shows the energy variation with the compression of the intersheet distance, which was obtained by fixing the length of the *c* axis and optimizing all the internal coordinates. The global minimum is located at ~11 Å, in agreement with what would be expected from the van der Waals radii of the clay and the C_{60} atoms. The left-hand side of the total energy variation with the compression of the molecule closely follows a parabola and, at the short distance observed experimentally, reaches a few hundred kilocalories per mole. It can be concluded that the calculations support the simplest explanation for the observed short interlayer distance, that is, the experiments provide an average distance due to filled and unfilled silicate layers.

The calculations also allow us to obtain the binding energy, E_b, of C_{60} to the clay platelets, which is obtained as

$$E_b = E_{tot} - E_{clay} - E_{C60} - E_{split} \quad (1)$$

where E_{tot} is the total energy of the optimized cell at a given value of the *c* axis, E_{clay} and E_{C60} are the contributions of the clay and C_{60} to the total energy, and E_{split} is the energy required to separate the two clay platelets between which the molecule is intercalated.

Figure 8b shows the energy trend, which appears to be nearly parabolic. The oscillations are caused by the variations of the structural parameters of the clay "hexagon" that hosts C_{60} (see Figure S2 in the Supporting Information). Such variations are reported in Table S1 in the Supporting Information (please notice that the symmetry of C_{60} and its nearly free rotation, also in its own solid, make the distinction between the two layers and the different atoms impossible). The data in Table S1 in the Supporting Information explain, for instance, the largest dip from the parabolic behavior in Figure 8b that is observed at 7.61 Å. This is brought about by the Si–O bond lengths that start to exceed their bulk value by a sizable amount (>1.7 Å); conversely, the Si–O–Si bond angles are much more flexible and do not appear to give rise to E_b discontinuities.

To assess the frequency shift of 7 cm^{-1} observed for the $A_g(2)$ mode, which is usually observed in singly charged fullerenes, we decided to obtain the total molecular charge of C_{60} in the clay with the charge equilibration, QEq, scheme of Rappe and Goddard.[24] The model assumes that the electronegativity of an atom depends on its "intrinsic" value and on a term that varies as a function of the charges and nature of the environment. In practice, the charge distribution within the system is calculated by solving a set of equations, which equilibrate charges and electronegativity via the Coulombic interactions between sites. The model has been previously successfully used to calculate geometry-dependent atomic charges in molecules and solids. It was created with the purpose of assigning sensible atomic charges and to reproduce realistic electric fields for modeling of complex systems such as phase transitions in SiO_2[25] and clays.[26] Figure 8c displays the variation of the C_{60} charge with the intersheet separation. At the equilibrium distance the molecular charge is ~−1.6, a value that fully justifies the shift observed in the Raman spectrum. Interestingly, as the platelet separation diminishes, the charge decreases. To explain this feature, we plotted the charges as a function of the molecule aspect ratio, that is, the ratio of the shortest and the longest radii. Figure 8d shows that total charge and aspect ratio correlate reasonably well.

Conclusions

In conclusion, we have described the insertion and the subsequent behavior of fulleropyrrolidine derivatives into the interlayer space of an aluminosilicate-layered material. A neutral derivative, with the help of the solvent, can be inserted and entrapped between the clay layers, affording a stable composite. The insertion of ionic fullerene derivatives was easier because of their solubility in water. Furthermore, it is important to note that the only significant change that takes place in the electronic properties of the fullerene is the presence of a negative charge on the molecule. The composites were characterized by several methods and constitute a new hybrid system where C_{60} differs from its crystals or its solutions.

Acknowledgment. This work was supported from the European Union through the Research Training Network "CASSIUS-CLAYS", contract HPRN CT-2002-00178 and MIUR (PRIN 2002, Prot. No. 2002032171). We would like to acknowledge the use of the XRD unit of the Laboratory Network, UOI.

Supporting Information Available: Simulation of clay–C_{60} intercalation, the clay hexagon hosting C_{60}, and table of calculated structural parameters of the clay hexagon hosting C_{60} (PDF). This material is available free of charge via the Internet at http://pubs.acs.org.

JA049237B

Baxter, R. J.; Teobaldi, G.; Zerbetto, F. *Langmuir* **2003**, *19*, 7335–7340.

(24) Rappe, A. K.; Goddard, W. A. *J. Phys. Chem.* **1991**, *95*, 3358.
(25) Demiralp, E.; Cagin, T.; Goddard, W. A. *Phys. Rev. Lett.* **1999**, *82*, 1708.
(26) Hwang, S. G.; Blanco, M.; Demiralp, E.; Cagin, T.; Goddard, W. A. *J. Phys. Chem. B* **2001**, *105*, 4122–4127.